Available online at www.sciencedirect.com
SCIENCE DIRECT®
Journal of Molecular Spectroscopy 219 (2003) 1–12
Journal of MOLECULAR SPECTROSCOPY
www.elsevier.com/locate/jms

Fourier transform spectroscopy of chemiluminescence from the $A'^1\Pi$–$X^1\Sigma^+$ system of SrO☆

Randall H. Skelton,[a] Hongzhi Li,[a] Chris D. Boone,[a] Robert J. Le Roy,[a,*] Peter F. Bernath,[a] Cristian Focsa,[b] and Bernard Pinchemel[b]

[a] *Department of Chemistry, University of Waterloo, Waterloo, Ont., Canada, N2L 3G1*
[b] *Laboratorie de Physique des Lasers, Atomes et Molécules, UMR CNRS, Center d'Etudes et de Recherches Lasers et Applications, Université des Sciences et Technologies de Lille, 59 655 Villeneuve d'Ascq cedex, France*

Received 26 December 2000; in revised form 22 October 2002

Abstract

The $A'^1\Pi$–$X^1\Sigma^+$ near infrared system of strontium oxide (SrO) was observed at high spectral resolution by measuring the chemiluminescence from a Broida flow reactor using a Fourier transform spectrometer. In total, 32 bands from ^{88}SrO, ^{87}SrO, ^{86}SrO were measured within the 4000–10 000 cm^{-1} spectral region at a resolution of 0.03 cm^{-1}. Vibrational levels of the upper state were observed up to $v_{A'} = 4$, and more than 5600 rotational lines were assigned. Incorporating previously published high resolution data for the $A^1\Sigma^+$–$X^1\Sigma^+$ system, a global fit to both data sets yields improved Dunham constants for the ground state and for the lower vibrational levels ($v_{A'} = 0$, 1, and 2) of the $A'^1\Pi$ state. Because perturbations arising from interactions with the $b^3\Sigma^+$ and $A^1\Sigma^+$ states affect the higher vibrational levels of the $A'^1\Pi$ state more strongly, levels $v_{A'} = 3$ and 4 were represented by effective band constants in the fits. RKR potentials for the $X^1\Sigma^+$, $A'^1\Pi$, and $b^3\Sigma^+$ states have been generated utilizing all the available data, Franck–Condon factors have been calculated for the $A'^1\Pi$–$X^1\Sigma^+$ system, and $A'^1\Pi \sim b^3\Sigma^+$ and $A'^1\Pi \sim A^1\Sigma^+$ perturbations are discussed.

1. Introduction

There has been a long standing interest in the electronic properties of alkaline earth oxides. The first spectroscopic investigation of SrO in the gas phase was undertaken in 1928 by Mecke and Guillery when they recorded a few bands belonging to the $B'^1\Pi - X^1\Sigma^+$ transition [1]. Shortly thereafter, Querbach [2], Mahla [3], and Meggers [4] reported observations of the $A^1\Sigma^+$–$X^1\Sigma^+$ band system in various spectral regions. Nearly two decades later, Lagerqvist et al. [5–7] reported an extensive rotational analysis of the $A^1\Sigma^+$–$X^1\Sigma^+$ system. In the 1970s, a resurgence of interest in the electronic spectra of the alkaline earth oxides yielded a plethora of papers, many of which involved low resolution spectra and examined chemiluminescence of metal vapour plus oxidant reactions. For example, Zare et al. [8,9] reported laser-induced fluorescence studies on BaO, SrO, CaO, and MgO in an effort to determine the reaction mechanisms of the alkaline metals with NO_2 and N_2O.

The $A'^1\Pi$ state of SrO was first investigated by Field [10] through his interpretation of the perturbations in the $A^1\Sigma^+$–$X^1\Sigma^+$ transition observed by Lagerqvist. The following year, a low resolution study of the $A'^1\Pi$–$X^1\Sigma^+$ system was reported [11], which yielded band constants of modest accuracy. In both of these publications the vibrational assignment was uncertain, and two proposed numbering schemes were suggested. Shortly afterwards, that ambiguity was resolved by Hecht [12] through a vibrational analysis of $Sr^{18}O$.

While practical applications of strontium oxide are currently limited, both the neutral and positive ions of the alkaline earth oxides exist in flames [13], stellar atmospheres [14], and magnetohydrodynamic plasmas [15]. The evaporation products of solid barium and strontium oxides also have important implications for

☆ Supplementary data for this article are available on ScienceDirect.

* Corresponding author. Fax: +519-746-0435.
E-mail address: leroy@uwaterloo.ca (R.J. Le Roy).

0022-2852/03/$ - see front matter © 2003 Elsevier Science (USA). All rights reserved.
doi:10.1016/S0022-2852(03)00006-7

the understanding of electron emission from oxide-coated cathodes [16].

This paper presents a near-infrared spectrum of SrO recorded using a Fourier transform spectrometer in which the $A'^1\Pi$–$X^1\Sigma^+$ system is observed for the first time at high resolution in the $4000 - 10\,000\,cm^{-1}$ spectral range. Our work is part of a series of papers investigating the emission spectra of CaO [17], SrO [18], and BaO [19]. The $A^1\Sigma^+$–$X^1\Sigma^+$ system of SrO was also observed, and has been reported elsewhere [18]. In contrast to recent results from our laboratory regarding CaO [17], which exhibits global perturbations from the $b^3\Sigma^+$ state alone, the $A'^1\Pi$ state of SrO is strongly affected both by homogeneous perturbations due to the $b^3\Sigma^+$ state and by heterogeneous perturbations due to the $A^1\Sigma^+$ state. Despite such perturbations, we have performed a combined analysis of the data for all the observed vibrational levels for the $A'^1\Pi$–$X^1\Sigma^+$ system, using band constants for the more strongly perturbed vibrational levels ($v_{A'} = 3$ and 4) and a Dunham representation elsewhere. To achieve the most comprehensive and reliable set of constants for the ground state, we have included high-resolution data for the $A^1\Sigma^+$–$X^1\Sigma^+$ system [18] as well as the available infrared and microwave measurements for the ground state [20,21]. From an analysis of the perturbations observed in the $A^1\Sigma^+$–$X^1\Sigma^+$ system, approximate band constants for higher vibrational levels of the $A'^1\Pi$ state have also been determined and used in the analysis.

Combining the present results with our recent data for the $X^1\Sigma^+$ state [18], with less accurate earlier data for higher vibrational levels of the $A'^1\Pi$ state [11], and with earlier published results for the $b^3\Sigma^+$ and $A^1\Sigma^+$, we have constructed Rydberg–Klein–Rees (RKR) potential energy functions for these four states. Using wavefunctions determined from these potentials, Franck–Condon factors were calculated for the $A'^1\Pi$–$X^1\Sigma^+$ and $A'^1\Pi$–$b^3\Sigma^+$ systems in an attempt to rationalize the observed band intensities and the global perturbations. Using these potentials, matrix elements of $1/r^2$ were generated and used to estimate the Λ-doubling parameters associated with the $A'^1\Pi \sim A^1\Sigma^+$ interaction.

2. Experimental

The SrO chemiluminescence was generated in a Broida-type oven [22] by the metal-oxidant reaction,

$$Sr + N_2O \rightarrow SrO + N_2 \quad (1)$$

Strontium atoms were produced by partial vaporization of a sample (~ 3 g) of the metal placed in an alumina crucible which was heated by a tungsten wire basket heater with a current of about 40 A. Argon carrier gas, typically at a pressure of 1–5 Torr, entered near the top of the crucible and entrained the strontium vapor, carrying it up into the reaction chamber. Both the argon and N_2O pressures were optimized to yield suitable spectra by monitoring low resolution scans.

A Bruker IFS 120 HR Fourier transform spectrometer (FTS), modified to record double-sided interferograms, was used to record the broadband chemiluminescence. The emission was focused onto the entrance aperture of the FTS by two CaF_2 lenses. A spherical mirror was placed on the opposite side of the flame, resulting in a gain of as much as 30% in the observed signal.

An InSb detector was used to cover the 1800–$10\,000\,cm^{-1}$ spectral region, while between 10 000–$16\,000\,cm^{-1}$ a silicon photodiode was used. The 1800–$10\,000\,cm^{-1}$ region was split into two parts using red- and blue-pass filters to give 1800–$6600\,cm^{-1}$ and 5300–$10\,000\,cm^{-1}$ regions, respectively. The instrument resolution was set to $0.03\,cm^{-1}$, and a total of 100 scans were co-added for each measurement.

The line positions were measured by fitting Voigt lineshape functions to the experimental lines in a non-linear least-squares procedure using the WSpectra program written by Dr. Michel Carleer of the Université Libre de Bruxelles. The precision of our measurements is estimated to be $\pm 0.005\,cm^{-1}$ for medium and strong unblended lines. To ensure that a satisfactory lineshape fit was achieved, a zero-filling factor [23] of 8 was applied to all recorded spectra. The air-to-vacuum conversion of the measured line positions was done by Edlén's formula [24,25]. The absolute wavenumber calibration was achieved using strong atomic Sr lines observed in the 3000–$5000\,cm^{-1}$ region [26]. Spectra recorded in the 5300–$10\,000\,cm^{-1}$ region were calibrated onto the same wavenumber scale using more than 100 lines from the (0,5) and (0,6) bands that were common to both measurements. Accordingly, we estimate the absolute accuracy of the wavenumber scale to be $\pm 0.005\,cm^{-1}$.

3. Results

3.1. Measurements and assignments

Visible and near infrared chemiluminescence from reactions of strontium with N_2O at low to moderate carrier-gas pressures consists of radiation from both A–X and A'–X band systems. Although pressure dependent emission has been reported in BaO generated with a Broida oven source [22], no large pressure effects were observed in our experiments. The relative intensities within the $Sr + N_2O$ spectrum appeared only slightly dependent on reactant concentration. This weak dependence is likely because of the large excess of buffer-gas atoms over reactant species.

An overview spectrum of the transition observed between 4000 and $14\,000\,cm^{-1}$ is displayed in Fig. 1. Both $A'^1\Pi$–$X^1\Sigma^+$ and $A^1\Sigma^+$–$X^1\Sigma^+$ bands are observed in

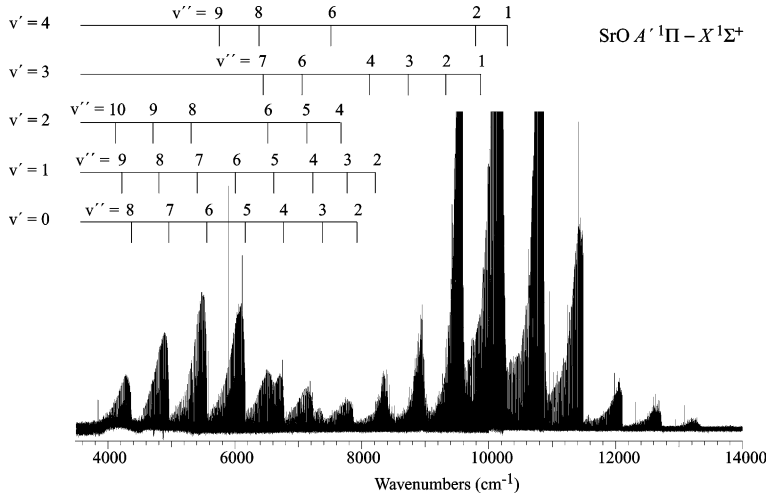

Fig. 1. Overview of the $A'^1\Pi$–$X^1\Sigma^+$ chemiluminescence spectrum of SrO recorded by Fourier transform spectroscopy showing vibrational band assignments. Unlabeled band are due to the $A^1\Sigma^+$–$X^1\Sigma^+$ system discussed in [18].

our chemiluminescence spectra, with the A'–X system predominant below 8500 cm^{-1} and the A–X system above 8500 cm^{-1}. Vibrational assignments for all of the observed bands of the $A'^1\Pi$–$X^1\Sigma^+$ system are also shown in this figure. More than 30 bands were identified, involving the $0 \leqslant v_{A'} \leqslant 4$ vibrational levels of the $A'^1\Pi$ state and vibrational levels $1 \leqslant v_X \leqslant 10$ of the $X^1\Sigma^+$ ground state. Although not visible in this plot, the minor isotopes of strontium ($^{87}Sr \sim 7.00\%$ and $^{86}Sr \sim 9.86\%$ in natural abundance) were also observed for the stronger $v_{A'} = 0$ and 1 bands.

The rotational assignment of lines for lower vibrational levels of the $A'^1\Pi$ state was quite simple, as no position or intensity perturbations were observed for $0 \leqslant v_{A'} \leqslant 2$. The expanded portion of the (0,6) band shown in Fig. 2 shows the expected P–Q–R structure that is typical of a $^1\Pi - {}^1\Sigma$ transition. For these bands, a Loomis–Wood program was used to select quickly the branches. Two additional tools proved quite useful in making these assignments. Firstly, the combination difference relationship

$$\Delta_2 F''(J) = P_v(J+1) - R_v(J-1) \approx 4B_v\left(J+\frac{1}{2}\right) - 8D_v\left(J+\frac{1}{2}\right)^3 \quad (2)$$

was often exploited to predict the lines of one branch, providing those of its partner had been assigned. In Eq.

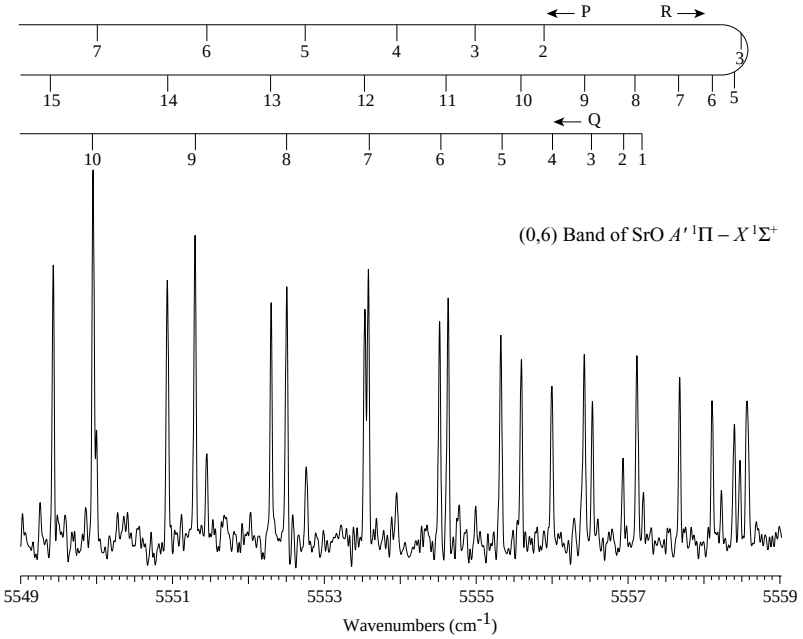

Fig. 2. Band-head region of the $A'^1\Pi$–$X^1\Sigma^+$ chemiluminescence spectrum of SrO for the (0,6) band.

(2) the symbol Δ indicates a difference between line positions represented by the standard $F(J)$ formulas, and its subscript 2 signifies that $\Delta J = 2$ for the differences. Secondly, in the absence of perturbations, for a vibrational progression (v', v'') from a given excited state v', each band in the progression can be predicted for a specific assigned lower level, $v''_{\rm ass}$ [19]

$$T''(v,J) - T''(v_{\rm ass},J) \approx G''_v - G''_{v_{\rm ass}} + \left(B''_v - B''_{v_{\rm ass}}\right) \times [J(J+1)] - \left(D''_v - D''_{v_{\rm ass}}\right) \times [J(J+1)]^2. \quad (3)$$

3.2. Strategy for the parameter-fit analysis

The present analysis was performed using program DSParFit [27], which allows spectroscopic data involving one or more isotopomers and one or more electronic states to be fitted to a variety of parameterized energy level expressions. Moreover, as is done in the present analysis, different energy representations can be used for different states and/or subsets of the data. This feature is particularly useful when fitting perturbed data sets or simultaneously fitting data for multiple electronic states. Regardless of the representation(s) used, each experimental datum is weighted by the inverse square of its estimated uncertainty. The quality of the fit is quantified by a dimensionless standard error $\overline{\sigma}_f$, which has a value of $\lesssim 1$ when on average the deviations from the model are within the estimated experimental uncertainties.

In order to obtain an optimum description of the ground state, our analysis consisted of a simultaneous fit to 5623 rovibrational lines from our new measurements for the $A'^1\Pi$–$X^1\Sigma^+$ system, 9047 rovibrational lines from the $A^1\Sigma^+$–$X^1\Sigma^+$ study of [18], 29 microwave data [20], and 43 infrared transitions [21]. With only a few exceptions for the weak branches involving $v_{A'} = 3$ and 4, the uncertainties of our new $A' - X$ data were set as $0.005\,{\rm cm}^{-1}$, while those of the other high-resolution data were taken as published.

For isotopomer α, the rovibrational energies of the $X^1\Sigma^+$ state and for most levels of the $A'^1\Pi$ state were represented by the conventional Dunham-type expansion [28],

$$E^{(\alpha)}(v,J) = \sum_{(m,l)\neq(0,0)} Y^{(\alpha)}_{l,m}\left(v+\frac{1}{2}\right)^l [J(J+1)-\Lambda^2]^m, \quad (4)$$

where $\Lambda = 0$ and 1 for the X and A' states, respectively, and constants for the various isotopomers were related to those for a selected reference isotopomer, $\alpha = 1$, through the conventional first-order semiclassical reduced mass scaling relationship

$$Y^{(\alpha)}_{l,m} = Y^{(1)}_{l,m}[\mu_1/\mu_\alpha]^{m+l/2}. \quad (5)$$

Note that the constants for the chosen reference isotopomer, here the most abundant species $^{88}{\rm Sr}^{16}{\rm O}$, are the only free parameters in the fit.

Because of the strength of global band perturbations, data involving levels $v_{A'} = 3$ and 4 could not be represented by this combined-isotopomer expression, and hence represented using band-constant expansions of the form:

$$E^{(\alpha)}(v,J) = \sum_{m=0} K^{(\alpha)}_m [J(J+1)-\Lambda^2]^m. \quad (6)$$

In this case, an independent set of band constants $\{K^{(\alpha)}_m = T^{(\alpha)}_v, B^{(\alpha)}_v, -D^{(\alpha)}_v, \ldots\}$ has to be determined for each vibrational level of each isotopomer α.

The degeneracy of rotational levels in the $A'^1\Pi$ state is lifted by Λ-doubling, which splits levels of e and f parity, and it may be represented in the fitting procedure by an additive correction in either a band-constant or Dunham-type representation,

$$\delta E^{(\alpha),\{e,f\}}_\Lambda = \pm\frac{1}{2}\sum_{m=1} q^{(\alpha)}_m(v)[J(J+1)-\Lambda^2]^m, \quad (7)$$

$$= \pm\frac{1}{2}\sum_{m=1}\left(\sum_{l=0} q^{(\alpha)}_{l,m}\left(v+\frac{1}{2}\right)^l\right)[J(J+1)-\Lambda^2]^m, \quad (8)$$

$$= \pm\frac{1}{2}\sum_{m=1}\left(\sum_{l=0}[\mu_1/\mu_\alpha]^{m+1+l/2} q^{(1)}_{l,m}\left(v+\frac{1}{2}\right)^l\right) \times [J(J+1)-\Lambda^2]^m, \quad (9)$$

where the + and − signs correspond to the e and f parity sublevels, respectively. In our band-constant fits for $v_{A'} = 3$ and 4, individual vibrational Λ-doubling parameters $q^{(\alpha)}_m(v)$ from Eq. (7) are determined for each vibrational level of each isotopomer, while for levels $v_{A'} = 0 - 2$ whose vibration–rotation energies are represented by the Dunham expansions of Eq. (4), the Dunham-like expression of Eq. (9) is used.

Properties of a number of the higher vibrational levels of the $A'^1\Pi$ state were obtained from the preliminary deperturbation analysis of $A^1\Sigma^+$-state term values described in the following subsection. Although the associated level energies and rotational constants are much less well determined than those for lower $v_{A'}$, they yield useful information in a region for which more accurate results are not yet available, so together with some earlier low resolution results from [11], they were utilized in the global data analysis of Section 3.4.

Our recent A–X analysis [18] reported the presence of sharp, J-dependent perturbations due to interactions of the $A^1\Sigma^+$ state with the $A'^1\Pi$ state and with the three spin components of the $a^3\Pi$ state. The strong perturbations in the A state are well known, and have been discussed at length in previous publications [10,29]. As in [18], in order to prevent the perturbations in the A

state from affecting our X-state constants, the present work combined an Åslund-type term-value representation [30–32] for the levels of the A-state with a conventional Dunham expression for the unperturbed X-state levels, using the equation (for isotopomer α)

$$\bar{\nu} = T_A^{(\alpha)}(v', J') - \sum_{(m,l)\neq(0,0)} Y_{l,m}^{(\alpha)} \left(v'' + \frac{1}{2}\right)^l [J''(J''+1)]^m, \tag{10}$$

where $\bar{\nu}$ is a line position and $T_A^{(\alpha)}$ is an A-state term value. In effect, the data from the $A^1\Sigma^+$–$X^1\Sigma^+$ system was treated as fluorescence series from individual A-state rovibronic energy levels. This approach yields a set of well-determined energy levels for the A state, and these term values are used in our deperturbation analysis to determine constants for some of the higher vibrational levels of the A' state (Section 3.3). However, no attempt was made to fit conventional molecular level energy expressions to these A-state level energies. As mentioned above, the X-state molecular constants for the different isotopomers are related by Eq. (5), and only those for the reference isotopomer ($\alpha = 1$) ^{88}SrO are free parameters in the fit.

3.3. Properties of the Π state derived from $A^1\Sigma^+$–$X^1\Sigma^+$ transitions

A preliminary deperturbation analysis of the $A^1\Sigma^+$ state term values obtained in the work of [18] has been used to determine approximate energies and inertial rotational constants for a number of the higher vibrational levels of the $A'^1\Pi$ state. In particular a number of independent small matrices were used to approximate the $A'^1\Pi - A^1\Sigma^+$ interaction in terms of coupling between neighbouring vibrational levels. These matrices typically involve one $A'^1\Pi$ level and two $A^1\Sigma^+$ vibrational levels. As discussed by Field [10], the non-zero off-diagonal elements between A' and A states are written as

$$\begin{aligned}
&\left\langle v_{A'}, J^e; A'^1\Pi|\widehat{H}'|v_A, J^e; A^1\Sigma^+\right\rangle \\
&\quad = -\left\langle v_A, J^e; A'^1\Pi|B(\widehat{J}_+\widehat{L}_- + \widehat{J}_-\widehat{L}_+)|v_{A'}, J^e; A^1\Sigma^+\right\rangle \\
&\quad = -\sqrt{2}b[J(J+1)]^{1/2}\langle v_A|B|v_{A'}\rangle,
\end{aligned} \tag{11}$$

where $B = B(r) = \hbar^2/2\mu r^2$ is in cm^{-1} and the (dimensionless) electronic factor $b = \langle A'|\widehat{L}_+|A\rangle$ is assumed to be $\sqrt{2}$, which is appropriate for a p orbital ($l = 1$) [10,45].

For each of the A'-state vibrational levels $v_{A'} = 5$–9, two near-resonant perturbations involving different vibrational levels in the A state were observed [18]. For example, vibrational level $v_{A'} = 5$ is perturbed by $v_A = 0$ at $J = 114$ and by $v_A = 1$ at $J = 47$. Using a simple 3×3 Hamiltonian matrix with off-diagonal matrix elements given by Eq. (11) and the A state energy levels with J near the perturbation region, our fits determined the constants for A'-state levels shown in Table 1. However, for vibrational levels with $v_{A'} > 9$, only one perturbation with the A state was observed, so only a 2×2 Hamiltonian matrix which involved one $A'^1\Pi$ level and only one $A^1\Sigma^+$ level, could be used. In this case, only one of the spectral constants, B_v or G_v, could be determined from this type of analysis, while the other needed to be fixed in the fit. For these levels, therefore, G_v was fixed using data from Capelle et al. [11], and deperturbed intertial rotational constants (B_v's) for these higher vibrational levels were obtained here. These deperturbed constants for $v_{A'} > 9$ are listed in Table 2; they are not

Table 1
Properties of $A'^1\Pi$-state levels of ^{88}SrO determined by deperturbation of $A^1\Sigma^+$ term values assuming only an $A^1\Sigma^+ \sim A'^1\Pi$ interaction

$v_{A'}$	G_v[a]	B_v	$-D_v/10^{-7}$
5	11 613.72(40)	0.24712(20)	−2.892(150)
6	12 034.2(20)	0.2496(30)	−4.2949(12000)
7	12 504.3(60)	0.2438(30)	−3.0[b]
8	12 952.4(50)	0.2403(10)	−3.0[b]
9	13 382.0(80)	0.2362(100)	−3.0[b]

[a] Relative to $v = 0, J = 0$ of the $X^1\Sigma^+$ state.
[b] Assumed value.

Table 2
Lower-resolution supplemental data for higher vibrational levels of the $A'^1\Pi$ state of ^{88}SrO used in the present analysis

v	G_v[a]	B_v
4	—	0.2488(50)[c]
5	11614(10)[b]	0.2471(50)[b]
	—	0.2468(50)[c]
	—	0.2479(50)[c]
6	12034(10)[b]	0.2496(50)[b]
	—	0.2456(50)[c]
7	12504(10)[b]	0.2438(50)[b]
	12504.6(50)[c]	0.2443(50)[c]
	12507.6(50)[c]	
8	12952(10)[b]	0.2403(50)[b]
	12943.0(50)[c]	0.2424(50)[c]
	12947.0(50)[c]	0.2421(50)[c]
9	13382(10)[b]	0.2362(50)[b]
	13378.2(50)[c]	0.2405(50)[c]
	—	0.2337(50)[c]
10	13812.4(50)[c]	—
11	14237.0(50)[c]	0.2369(50)[b]
12	14657.2(50)[c]	0.2369(50)[b]
	14665.2(50)[c]	—
13	15080.2(50)[c]	—
14	15496.9(50)[c]	—
15	15905.4(50)[c]	0.2305(50)[b]
16	16313.8(50)[c]	—
17	16711.1(50)[c]	—
18	17114.4(50)[c]	—

The assumed uncertainties in the last significant digits shown are given in brackets, and all quantities have units cm^{-1}.
[a] Relative to $v = 0, J = 0$ of the $X^1\Sigma^+$ state.
[b] Deperturbation of the $A^1\Sigma^+$–$X^1\Sigma^+$ system (Section 3.3 and Table 1).
[c] Data from Capelle et al. [11].

very accurate, but they allow determination of a more realistic extended RKR potential than would otherwise be possible. Note that only $A \sim A'$ interactions were considered in this deperturbation analysis.

3.4. Recommended molecular constants for the $A'^1\Pi$ and $X^1\Sigma^+$ states of SrO

As was mentioned above, our final global fit simultaneously treated all of the new high resolution $A'^1\Pi - X^1\Sigma^+$ data reported herein, together with the $A^1\Sigma^+ - X^1\Sigma^+$ data of [18] and earlier microwave and infrared data for the ground state, for all three isotopomers. In addition, in order to yield the most extensive possible description of the $A'^1\Pi$ state, the input data set also included the deperturbed A'-state level properties discussed in Section 3.3 and the earlier results of Capelle et al. [11] listed in Table 2. The much larger uncertainties associated with these data mean that their inclusion will not compromise the accuracy of our Dunham constants for $v_{A'} = 0 - 2$ and band constants for $v_{A'} = 3$ and 4. At the same time, they will yield a more realistic estimate of the upper part of the A'-state potential energy well.

Note that the uncertainties used to weight the lower resolution Table 2 data in the global fit (numbers in parentheses) differ from those determined in the deperturbation fits of Section 3.3 or reported in [11]. Although each of these quantities had an uncertainty associated with its determination, those uncertainties proved to be unrealistically small when attempting to represent all of the data for the $A'^1\Pi$ state over the desired vibrational energy range. Hence, these data were reweighted using the uncertainties shown in Table 2, depending on the manner in which they were determined (i.e., directly observed, deperturbation alone, or deperturbation using additional information). With regard to the low resolution data from Capelle et al. [11], despite the small separation between band heads and origins, a more conservative uncertainty estimate of $5\,\mathrm{cm}^{-1}$ has been used for their band-head positions. For the rotational data presented in their work, a combination of a deperturbation analysis for the $A^1\Sigma^+$–$X^1\Sigma^+$ system and band-head data for the $A'^1\Pi$–$X^1\Sigma^+$ system provided moderately accurate constants. Nevertheless, these estimated uncertainties in their B_v values have been relaxed to $0.005\,\mathrm{cm}^{-1}$ in the present analysis (see Table 2).

In the final fit, a total of 16 Dunham constants were required to represent the $X^1\Sigma^+$ state (as in [18]), and 26 Dunham-type vibration–rotation and Λ-doubling constants to represent the A' state for $v_{A'} = 0 - 18$. Optimum representations of the $v_{A'} = 3$ and 4 levels required four band constants and three Λ-doubling constants for each vibrational level, and values were obtained only for ^{88}SrO. The dimensionless standard error of the global fit to all 15 979 data was 1.95. The resulting parameters for the $X^1\Sigma^+$ and $A'^1\Pi$ states, and their 95% confidence limit uncertainties, are presented in Tables 3 and 4, respectively. These results were obtained using a sequential rounding and refitting procedure which yields a final parameter set involving a minimum number of significant digits with no loss in accuracy in the predictions they provide [33]. The Dunham constants for the minor isotopomers ^{87}SrO and ^{86}SrO were generated using Eq. (5), and are also listed in these tables.

In addition to the molecular parameters presented in Tables 3 and 4, this analysis yields 1317 unbiased term values for levels of the $A^1\Sigma^+$ state: 981 for ^{88}SrO levels ranging from $v_A = 0 - 8$ with J values from 0 to 50, 137 for ^{87}SrO levels involving $v_A = 0 - 3$, and 199 for ^{86}SrO levels involving $v_A = 2$ and 3. These term values were the basis for the deperturbation analysis of Section 3.3, and will be basic input for any more comprehensive analysis of this system. These term values, together with the experimental data used in the analysis and a listing of the final [calc. – obs.] discrepancies are available from the Journal's online data archive.

3.5. Franck–Condon factors and matrix elements for the $A'^1\Pi$–$X^1\Sigma^+$ and $A'^1\Pi$–$b^3\Sigma^+$ systems

The potential energy curves and Franck–Condon factors reported herein were generated using computer programs RKR1 [34] and LEVEL [35]. RKR1 utilizes the first-order semiclassical RKR inversion procedure to determine the potential energy function of a diatomic molecule from a knowledge of the v-dependence of its vibrational level energies G_v and inertial rotational constants B_v. This approach was found to be quite accurate in the case of SrO due to its fairly large reduced mass, and quantum mechanical eigenvalues and rotational constants numerically calculated from the result-

Table 3
Molecular constants (in cm^{-1}) for the ground state of SrO

Constant	^{88}SrO	^{87}SrO	^{86}SrO
$Y_{1,0}$	653.30834 (170)	653.8848096	654.4758527
$Y_{2,0}$	−3.84992 (90)	−3.85671722	−3.86369251
$Y_{3,0}$	−0.02025 (20)	−0.020303652	−0.020358759
$10^3 \times Y_{4,0}$	1.2956 (180)	1.3001789	1.3048862
$10^3 \times Y_{5,0}$	−0.0101 (6)	−0.01014464	−0.01019057
$Y_{0,1}$	0.33797194 (16)	0.338568646	0.3391809835
$Y_{1,1}$	−0.00215595 (27)	−0.00216166217	−0.00216752922
$10^7 \times Y_{2,1}$	−197.43 (120)	−198.12276	−198.84508
$10^7 \times Y_{3,1}$	2.8 (2)	2.812375	2.825109
$10^7 \times Y_{4,1}$	0.1768 (88)	0.1777381	0.1787042
$10^7 \times Y_{0,2}$	−3.61094 (220)	−3.62370184	−3.6368214
$10^7 \times Y_{1,2}$	−0.0448 (2)	−0.044998	−0.04520174
$10^{11} \times Y_{2,2}$	−7.4 (6)	−7.43926	−7.4797
$10^{11} \times Y_{3,2}$	1.14 (6)	1.14706	1.15434
$10^{14} \times Y_{0,3}$	−6.15 (99)	−6.18263	−6.21624
$10^{14} \times Y_{1,3}$	−1.43 (5)	−1.43886	−1.44798

The numbers in parentheses are the 95% confidence limit uncertainties in the last significant digits shown, and the Dunham constants for the minority isotopomers were rounded at the first significant digit of the parameter sensitivity [33].

Table 4
Molecular constants (in cm^{-1}) determined for the $A'^1\Pi$ state of SrO

Constant	^{88}SrO	^{87}SrO	^{86}SrO
Dunham-type parameters			
T_{00}	9 312.4279 (13)	9 312.3500	9 312.2702
$Y_{1,0}$	476.4327 (1100)	476.853097	477.284122
$Y_{2,0}$	−3.6114 (890)	−3.6177761	−3.6243192
$Y_{3,0}$	0.164 (23)	0.1644345	0.1648808
$Y_{4,0}$	−0.005 (1)	−0.00501767	−0.00503584
$Y_{0,1}$	0.2572729 (130)	0.2577271279	0.2581932549
$10^3 \times Y_{1,1}$	−2.4249 (370)	−2.4313248	−2.4379237
$10^3 \times Y_{2,1}$	0.2173 (260)	0.218068	0.2188575
$10^3 \times Y_{3,1}$	−0.012 (6)	−0.01205304	−0.01210761
$10^7 \times Y_{0,2}$	−5.1924 (540)	−5.2107511	−5.2296165
$10^7 \times Y_{1,2}$	2.045 (100)	2.0540383	2.0633383
$10^7 \times Y_{2,2}$	−0.49 (3)	−0.4925999	−0.4952775
$10^{11} \times Y_{0,3}$	3.49 (14)	3.508518	3.527589
$10^{11} \times Y_{1,3}$	−3.06 (26)	−3.078951	−3.098485
$10^{11} \times Y_{2,3}$	0.679 (77)	0.6838079	0.6887683
$10^{15} \times Y_{0,4}$	−2.847 (160)	−2.867159	−2.887958
$10^{15} \times Y_{1,4}$	2.2228 (2500)	2.240515	2.258807
$10^{15} \times Y_{2,4}$	−0.42 (6)	−0.4237208	−0.4275664
$10^{20} \times Y_{0,5}$	8.1 (6)	8.17176	8.24592
$10^{20} \times Y_{1,5}$	−3.7 (8)	−3.73607	−3.77339
$10^6 \times q_{0,1}$	−8. (2)	−8.0283	−8.0573
$10^6 \times q_{1,1}$	−57.3 (38)	−57.5532	−57.8138
$10^6 \times q_{2,1}$	8.3 (15)	8.344	8.3894
$10^9 \times q_{0,2}$	−9.52 (36)	−9.5705	−9.6225
$10^9 \times q_{1,2}$	14.82 (79)	14.9118	15.0064
$10^9 \times q_{2,2}$	−3.9 (3)	−3.92762	−3.95611
Band constants ($v_{A'} = 3$ and 4)			
G_3	10706.1817 (23)[a]		
B_3	0.2505453 (52)		
$10^7 \times (-D_3)$	−2.742 (30)		
$10^{12} \times H_3$	−2.5 (5)		
$10^4 \times q_1(3)$	−2.936 (58)		
$10^8 \times q_2(3)$	5.23 (43)		
$10^{12} \times q_3(3)$	−4.3 (8)		
G_4	11162.032 (3)[a]		
B_4	0.249108 (13)		
$10^7 \times (-D_4)$	−2.98 (9)		
$10^{12} \times H_4$	6.0 (15)		
$10^4 \times q_1(4)$	1.54 (21)		
$10^8 \times q_2(4)$	1.0 (16)		
$10^{12} \times q_3(3)$	1.12 (29)		

The numbers in parentheses are the 95% confidence limit uncertainties in the last significant digits shown, and the Dunham constants for the minority isotopomers were rounded at the first significant digit of the parameter sensitivity [33].

[a] Energies relative to the ground state $v_X = 0$, $J_X = 0$ level of this isotopomer.

ing potentials agree within experimental error with our fit results. Program LEVEL determines the discrete eigenvalues and eigenfunctions of the radial Schrödinger equation from any given potential(s), together with any desired radial expectation values or matrix elements.

RKR turning-points for the $X^1\Sigma^+$ and $A'^1\Pi$ states were calculated using the Dunham expansion coefficients for G_v and B_v listed in Tables 3 and 4. Note, however, that more accurate descriptions of the data for levels $v_{A'} = 3$ and 4 are provided by the band constants listed in Table 4. The molecular constants used for the $A^1\Sigma^+$ state were taken from Huber and Herzberg [36]. Because of the difficulty of observing it, little is known about the $b^3\Sigma^+$ state, and only estimates for the band constants T_v, ω_e and B_v based on low resolution spectra have been published [37] (note that in Table VII of Herrmann et al. [37], the T_0 value of the $b^3\Sigma^+$ state should be 9883.53 cm^{-1}).[1] To generate a realistic RKR potential for this state, we adopted plausible estimates of 1.8 and 0.002 cm^{-1} for $\omega_e x_e$ and α_e, respectively. For convenience, the molecular constants used for the $A^1\Sigma^+$ and $b^3\Sigma^+$ states are listed in Table 5.

Figs. 3 and 4 schematically illustrate the potential curves and lower vibrational levels of the $X^1\Sigma^+, A'^1\Pi$, $A^1\Sigma^+$ and $b^3\Sigma^+$ states for SrO. The ground-state dissociation energy was set at the JANAF value [38], $\mathfrak{D}_{00} = 35\,650(\pm 1400)\,cm^{-1}$, as recommended by Partridge et al. [39], and the asymptotes for the other potentials are determined by the appropriate atomic excitation energies (see Fig. 3). Table 6 lists the Franck–Condon factors (upper entry for each band) and band origin energy differences $[E_{v'} - E_{v''}]$ (lower entry, in parentheses) calculated from the potentials for the $A'^1\Pi$–$X^1\Sigma^+$ system. An approximate Condon parabola is indicated on the table using bold-type. Note, that our predictions regarding which are the most intense bands differ somewhat from those reported by Field [10].

3.6. Estimations for the perturbations

In terms of molecular orbitals, the electronic structure of the lowest energy level of SrO is the closed-shell configuration $\cdots 9\sigma^2 10\sigma^2 4\pi^4 ({}^1\Sigma^+)$. The open-shell structures of low-lying excited states should have configurations representing excitation into the unoccupied 11σ and 5π orbitals [40–42].

$\cdots 9\sigma^2 10\sigma^2 4\pi^3 11\sigma^1$	$^3\Pi, ^1\Pi$
$\cdots 9\sigma^2 10\sigma^1 4\pi^4 11\sigma^1$	$^3\Sigma^+$, $^1\Sigma^+$
$\cdots 9\sigma^2 10\sigma^2 4\pi^2 11\sigma^2$	$^3\Sigma^-$, $^1\Sigma^+$, $^1\Delta$
$\cdots 9\sigma^2 10\sigma^2 4\pi^3 5\pi^1$	$^3\Sigma^+$, $^3\Delta$, $^3\Sigma^-$, $^1\Sigma^-$, $^1\Delta$, $^1\Sigma^-$
$\cdots 9\sigma^2 10\sigma^1 4\pi^4 5\pi^1$	$^3\Pi$, $^1\Pi$.

Using a simple ionic model due to Field and coworkers [43,44], a qualitative picture can be established for the electronic structure of many of these states. With the exception of the nominally divalent (Sr^{2+} O^{2-}) $X^1\Sigma^+$ state, all of the low-lying states of SrO can be characterized as a combination of Sr^+-centered orbitals (σ, π) and O^- p^{-1} electron holes (σ^{-1}, π^{-1}). For example, taking a Sr^+ atom with a singly filled s orbital (σ^1) and combining it with σp^{-1} creates the $A^1\Sigma^+$ and $b^3\Sigma^+$ states, while using the O^- πp^{-1} orbitals yields the $A'^1\Pi$ and $a^3\Pi$ states.

[1] W. Ernst, Private Communication, 2001.

Table 5
Constants used to generate RKR potentials for the $b^3\Sigma^+$ state (based on [37]), and the $A^1\Sigma^+$ state (from Huber and Herzberg [36]), all in cm^{-1}

Constant		$b^3\Sigma^+$	$A^1\Sigma^+$
	T_0	9 883.53	10 870.40
$Y_{1,0}$	ω_e	495.1	619.58
$Y_{2,0}$	$-\omega_e x_e$	−1.8	−0.89
$Y_{3,0}$	$\omega_e y_e$	—	−0.054
$Y_{0,1}$	B_e	0.2853(8)	0.30471
$Y_{1,1}$	$-\alpha_e$	−0.002	−0.00112

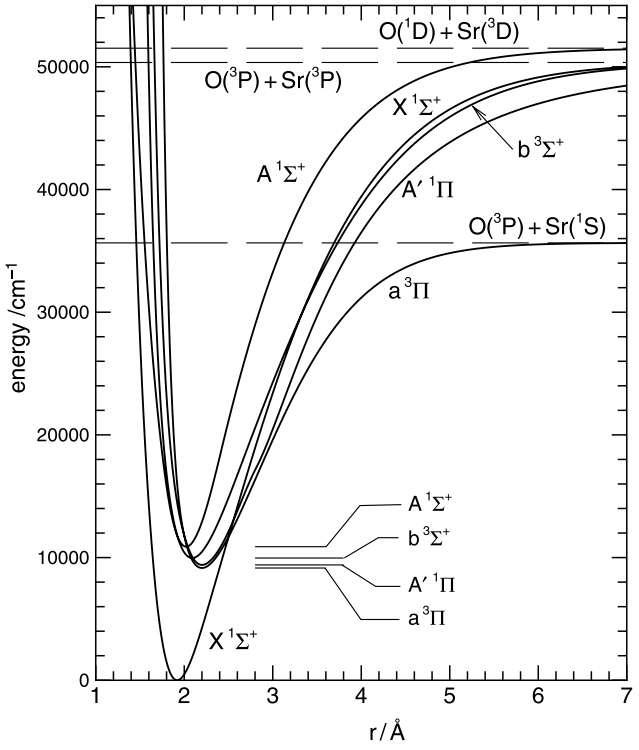

Fig. 3. Potential curves for the $X^1\Sigma^+, A'^1\Pi, b^3\Sigma^+, a^3\Pi$, and $A^1\Sigma^+$ states of SrO.

As in our recent work on CaO [17], the $v_{A'} = 0$, 1, and 2 levels of the $A'^1\Pi$ upper state are referred to as being "unperturbed," while the higher-v levels ($v_{A'} = 3$ and 4) are termed "perturbed." However, this terminology is not entirely accurate, since some of the band constants for $v_{A'} = 0 - 2$ have peculiar magnitudes. This means that our Dunham constants for the A' state are actually effective constants that have absorbed non-negligible perturbation effects. Unfortunately, no sharp, local perturbations were observed in the low vibrational levels of the $A'^1\Pi$ state. Given the limited range of vibrational and rotational levels observed, the absence of such local perturbations is expected (see Table III of [10]). On the other hand, as illustrated in Fig. 3, the potential curves for the $a^3\Pi$, $b^3\Sigma^+$ and $A^1\Sigma^+$ states all lie near the $A'^1\Pi$ state, and each of them can potentially interact with the $A'^1\Pi$ state to cause perturbations.

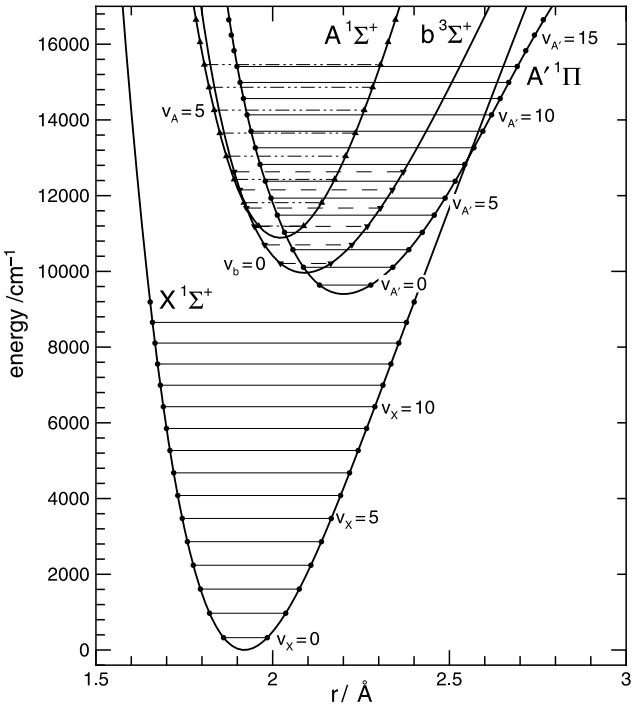

Fig. 4. An expanded region of the potential curves depicting the vibrational levels of the $X^1\Sigma^+, A'^1\Pi, b^3\Sigma^+$, and $A^1\Sigma^+$ states of SrO.

One possibility is that the A' state is homogeneously perturbed by spin–orbit interaction with either the $a^3\Pi$ or $b^3\Sigma^+$ states. Such an interaction can be described using the microscopic form of the spin–orbit operator [45]

$$\widehat{H}_{\rm so} = \sum_i a_i \widehat{\boldsymbol{l}}_i \cdot \widehat{\boldsymbol{s}}_i = \sum_i a_i \left(\widehat{l}_z \widehat{s}_z + \frac{1}{2}(\widehat{l}_+ \widehat{s}_- + \widehat{l}_- \widehat{s}_+) \right). \tag{12}$$

In terms of the electronic configuration of each atom, the $A'^1\Pi$ state is represented as $\mathrm{Sr}(\sigma^1)\mathrm{O}(p\pi^{-1})$, while the $b^3\Sigma^+$ state is $\mathrm{Sr}(\sigma^1)\mathrm{O}(p\sigma^{-1})$. Assuming that the $\mathrm{O}(p\sigma)$ and $\mathrm{O}(p\pi)$ orbitals can be represented as the oxygen p-orbitals (not necessarily an accurate approximation), the spin–orbit operator has a non-zero matrix element and perturbs the spectrum through terms of the form [45]

$$\begin{aligned} \widehat{H}_{v_b, v_{A'}} &= \left\langle v_b; b^3\Sigma^+ | \widehat{H}_{\rm so} | v_{A'}; A'^1\Pi \right\rangle \\ &= \left\langle v_b; {}^3\Sigma_1^+ p\sigma^{-1} | \frac{1}{2} a \widehat{l}_- \widehat{s}_+ | v_{A'}; {}^1\Pi p\pi^{-1} \right\rangle \\ &= \frac{a}{\sqrt{2}} \langle v_b | v_{A'} \rangle, \end{aligned} \tag{13}$$

where $\langle v_b | v_{A'} \rangle$ is the vibrational overlap integral. Note that the other spin component of the $b^3\Sigma^+$ state ($^3\Sigma_{0^-}^+$) cannot interact with the $A'^1\Pi$ state in this manner. An expression analogous to Eq. (13) can also be used to describe the $A'^1\Pi_1 \sim a^3\Pi_1$ interaction using the $\widehat{l}_z \widehat{s}_z$ component of the interaction Hamiltonian. However, as

Table 6
Franck–Condon factors (upper entry for each band) and the band origin energy differences $[E_{A'}(v'_A) - E_X(v_X)]$ (lower entry, in parentheses) for the $A'^1\Pi$–$X^1\Sigma^+$ system

$v_{A'} \setminus v_X$	0	1	2	3	4	5	6	7	8	9	10	11	12	13
0	0.0001	0.0017	0.0093	0.0318	0.0761	**0.1349**	**0.1831**	**0.1941**	**0.1631**	0.1094	0.0589	0.0255	0.0088	0.0024
	(9312.)	(8667.)	(8029.)	(7399.)	(6778.)	(6164.)	(5558.)	(4959.)	(4369.)	(3787.)	(3212.)	(2644.)	(2084.)	(1531.)
1	0.0010	0.0088	0.0359	0.0849	**0.1244**	0.1083	0.0424	0.0002	0.0362	**0.1150**	**0.1591**	**0.1394**	0.0864	0.0397
	(9782.)	(9136.)	(8499.)	(7869.)	(7247.)	(6633.)	(6027.)	(5429.)	(4839.)	(4256.)	(3681.)	(3114.)	(2554.)	(2001.)
2	0.0036	0.0248	0.0721	**0.1078**	0.0764	0.0112	0.0133	0.0753	0.0818	0.0207	0.0061	0.0766	**0.1446**	**0.1412**
	(10246.)	(9600.)	(8962.)	(8333.)	(7711.)	(7097.)	(6491.)	(5893.)	(5303.)	(4720.)	(4145.)	(3578.)	(3018.)	(2465.)
3	0.0093	0.0486	**0.0959**	0.0769	0.0105	0.0162	0.0697	0.0438	0.0000	0.0461	0.0815	0.0281	0.0038	0.0752
	(10704.)	(10059.)	(9421.)	(8791.)	(8170.)	(7556.)	(6950.)	(6352.)	(5761.)	(5179.)	(4604.)	(4036.)	(3476.)	(2923.)
4	0.0195	0.0739	**0.0901**	0.0248	0.0070	0.0593	0.0360	0.0010	0.0512	0.0484	0.0003	0.0435	0.0763	0.0188
	(11159.)	(10513.)	(9875.)	(9246.)	(8624.)	(8010.)	(7404.)	(6806.)	(6215.)	(5633.)	(5058.)	(4491.)	(3930.)	(3378.)
5	0.0341	**0.0906**	0.0578	0.0001	0.0430	0.0439	0.0000	0.0427	0.0375	0.0006	0.0499	0.0395	0.0007	0.0568
	(11609.)	(10963.)	(10326.)	(9696.)	(9074.)	(8460.)	(7854.)	(7256.)	(6666.)	(6083.)	(5508.)	(4941.)	(4381.)	(3828.)
6	0.0518	**0.0911**	0.0204	0.0155	0.0543	0.0054	0.0271	0.0405	0.0000	0.0425	0.0272	0.0053	0.0559	0.0204
	(12056.)	(11410.)	(10772.)	(10143.)	(9521.)	(8907.)	(8301.)	(7703.)	(7112.)	(6530.)	(5955.)	(5387.)	(4827.)	(4275.)
7	0.0698	**0.0748**	0.0008	0.0435	0.0282	0.0068	0.0453	0.0034	0.0296	0.0297	0.0033	0.0472	0.0099	0.0226
	(12499.)	(11853.)	(11216.)	(10586.)	(9964.)	(9350.)	(8744.)	(8146.)	(7556.)	(6973.)	(6398.)	(5831.)	(5271.)	(4718.)
8	**0.0846**	0.0484	0.0063	0.0521	0.0025	0.0341	0.0201	0.0110	0.0375	0.0000	0.0384	0.0122	0.0186	0.0401
	(12939.)	(12293.)	(11656.)	(11026.)	(10404.)	(9790.)	(9184.)	(8586.)	(7996.)	(7413.)	(6838.)	(6271.)	(5711.)	(5158.)
9	**0.0937**	0.0224	0.0265	0.0356	0.0054	0.0405	0.0001	0.0360	0.0070	0.0235	0.0223	0.0079	0.0379	0.0000
	(13376.)	(12730.)	(12093.)	(11463.)	(10841.)	(10227.)	(9621.)	(9023.)	(8433.)	(7850.)	(7275.)	(6708.)	(6148.)	(5595.)
10	**0.0959**	0.0053	0.0449	0.0120	0.0265	0.0199	0.0135	0.0276	0.0043	0.0334	0.0001	0.0349	0.0034	0.0290
	(13809.)	(13164.)	(12526.)	(11896.)	(11274.)	(10660.)	(10054.)	(9456.)	(8866.)	(8283.)	(7709.)	(7141.)	(6581.)	(6028.)
11	**0.0919**	0.0000	0.0505	0.0002	0.0397	0.0015	0.0329	0.0043	0.0267	0.0091	0.0202	0.0162	0.0127	0.0256
	(14239.)	(13593.)	(12956.)	(12326.)	(11704.)	(11090.)	(10484.)	(9886.)	(9296.)	(8713.)	(8138.)	(7571.)	(7011.)	(6458.)
12	0.0835	0.0048	0.0427	0.0052	0.0337	0.0043	0.0303	0.0029	0.0294	0.0014	0.0298	0.0002	0.0309	0.0002
	(14665.)	(14019.)	(13382.)	(12752.)	(12130.)	(11516.)	(10910.)	(10312.)	(9722.)	(9139.)	(8564.)	(7997.)	(7437.)	(6884.)
13	0.0726	0.0151	0.0278	0.0193	0.0168	0.0203	0.0123	0.0199	0.0105	0.0190	0.0104	0.0178	0.0117	0.0162
	(15086.)	(14441.)	(13803.)	(13173.)	(12551.)	(11938.)	(11332.)	(10733.)	(10143.)	(9561.)	(8986.)	(8418.)	(7858.)	(7305.)
14	0.0610	0.0267	0.0130	0.0318	0.0032	0.0315	0.0005	0.0296	0.0000	0.0278	0.0002	0.0267	0.0004	0.0268
	(15503.)	(14858.)	(14220.)	(13590.)	(12968.)	(12354.)	(11748.)	(11150.)	(10560.)	(9977.)	(9402.)	(8835.)	(8275.)	(7722.)
15	0.0499	0.0362	0.0033	0.0363	0.0004	0.0294	0.0042	0.0219	0.0088	0.0158	0.0125	0.0115	0.0155	0.0089
	(15914.)	(15269.)	(14631.)	(14001.)	(13379.)	(12766.)	(12160.)	(11561.)	(10971.)	(10389.)	(9814.)	(9246.)	(8686.)	(8133.)

Bold-font numbers approximate the Condon parabola.

is shown in Fig. 3, the potentials for these states are approximately parallel to each other, differing by only a small energy shift. Thus, the homogeneous interactions between vibrational levels should yield a nearly constant shift for all the vibrational levels in each electronic state.

Both the $A'^1\Pi \sim b^3\Sigma^+$ and $A'^1\Pi \sim a^3\Pi_1$ interactions are homogeneous (non-J dependent), and are strong because the molecular spin–orbit constant will be approximately the same as the O^- atom splitting constant, with $a = \zeta_{2p} = -121\,\mathrm{cm}^{-1}$ [45]. Eq. (13) shows that the strength of the interaction is directly proportional to the vibrational overlap integral. Hence, one may expect to find a correlation between the magnitudes of the $b^3\Sigma^+ - A'^1\Pi$ Franck–Condon factors and of global perturbations in the $v_{A'}$ levels observed in the $A'^1\Pi$–$X^1\Sigma^+$ system. As illustrated in Fig. 4, for $v_{A'} \geqslant 1$ the energy differences between neighbouring vibrational levels in the A' and b states increase as v increases.

To a first approximation, second-order perturbation theory can be used to predict the expected vibrational band shift in the A' state due to coupling to nearby b state vibrational levels:

$$\Delta E^{(2)}_{A'}(v_{A'}) = \frac{a^2}{2} \sum_{v_b} \frac{|\langle v_{A'}|v_b\rangle|^2}{E^{(0)}_{A'}(v_{A'}) - E^{(0)}_b(v_b)} \tag{14}$$

where $|\langle v_{A'}|v_b\rangle|^2$ is the Franck–Condon factor, and $E^{(0)}_b$ and $E^{(0)}_{A'}$ are the unperturbed energies [45]. Note that we are ignoring both any J dependence caused by centrifugal distortion in the interaction matrix element, and any J-dependent effects caused by the different B_v values in the two interacting states. In spite of the low quality of our knowledge of the $b^3\Sigma^+$ state, our application of Eq. (14) used sums with v_b ranging from 0 to 15 for each A' vibrational level, in order to achieve convergence. The resulting predicted displacements of the A' band origins are given in Table 7.

Consideration of the relative energies of levels of the b and A' states shown in Fig. 4 provides a good qualitative understanding of the $v_{A'}$-dependence of the predictions of Table 7. In particular, for $v_{A'} = 0$, all contributions to this sum are negative, and since the smallest level energy separation ($[E^{(0)}_{A'}(0) - E^{(0)}_b(0)] = -569\,\mathrm{cm}^{-1}$) is relatively large, the overall level shift is not too large. For $v_{A'} = 1$ all contributions are again negative, but the relatively close proximity of the nearest b-state level ($[E^{(0)}_{A'}(1) - E^{(0)}_b(0)] = -100\,\mathrm{cm}^{-1}$) makes its contribution to the predicted shift unusually large. In contrast, for higher $v_{A'}$ levels the magnitude of the perturbation becomes smaller again, both because all of the energy denominators are larger, and because the presence of b-state levels lying below as well as above a particular A'-state level gives rise to positive and negative term cancellations in the summation of Eq. (14). However, the prediction of a particularly large negative shift for level $v_{A'} = 1$ disagrees with our data, which suggests either that the available parameters used to generate the $b^3\Sigma^+$ state potential and Franck–Condon factors are not correct, or that our model for the perturbation is not valid, or both. Shifting the assumed [37] vibrational assignments by ± 1 does not remove this disagreement.

Table 7
Predicted vibrational band origin shifts for the $A'^1\Pi$ state due to the spin–orbit interaction with the $b^3\Sigma^+$ state

$v_{A'}$	Shift (cm^{-1})
0	−7.94
1	−25.91
2	−3.63
3	0.45
4	−2.29
5	−3.98
6	−3.36

Another type of perturbation affecting this system is the $A'^1\Pi \sim A^1\Sigma^+$ interaction which lifts the e/f degeneracy of A'-state rotational levels. As discussed above, the interaction of these states is known to perturb the A-state rotational levels, but corresponding perturbations in the A' state had not previously been reported. As seen in Fig. 4, the $v_A = 0$ vibrational level of the A state lies between the $v_{A'} = 3$ and 4 levels of the A' state, so relatively strong perturbations of these levels may be expected to occur. For a particular vibrational level in the $A'^1\Pi$ state, the shift due to perturbation from the $A^1\Sigma^+$ state can be calculated as a sum over contributions from all vibrational levels in the $A^1\Sigma^+$ state, where $\widehat{H}'$ is the same operator appearing in Eq. (11) [45]:

$$\Delta E^{(2)}_{A'}(v_{A'}, J^e) = \sum_{v_A} \frac{\left|\left\langle v_{A'}, J^e; A^1\Sigma^+|\widehat{H}'|v_A, J^e; A'^1\Pi\right\rangle\right|^2}{E^{(0)}_{A'}(v_{A'}, J^e) - E^{(0)}_A(v_A, J^e)} \tag{15}$$

$$= 4[J(J+1)] \sum_{v_A} \frac{|\langle v_{A'}, J^e|B|v_A, J^e\rangle|^2}{E^{(0)}_{A'}(v_{A'}, J^e) - E^{(0)}_A(v_A, J^e)}. \tag{16}$$

The value of the matrix element $\langle v_{A'}, J^e|B|v_A, J^e\rangle$ varies slowly as a function of J^e, and the denominator is approximately constant as a function of J^e. Neglecting this J-dependence, the inertial rotational constants for the e and f levels can be expressed in terms of the energy shift of Eq. (16):

$$B^e_v = B_v[J(J+1) - \Lambda^2] + q_{1v}[J(J+1)] \tag{17}$$

$$B^f_v = B_v[J(J+1) - \Lambda^2] \tag{18}$$

where the Λ-doubling constant q_v is

$$q_{1v} = 4 \sum_{v_A} \frac{|\langle v_{A'}|B|v_A\rangle|^2}{E^{(0)}_{A'}(v_{A'}) - E^{(0)}_A(v_A)}. \tag{19}$$

Table 8
Predicted and observed Λ-doubling constants (in cm^{-1}) due to interaction of the $A'^1\Pi$ and $A^1\Sigma^+$ states

$v_{A'}$	$10^5 \times q_{B1}(v_{A'})$ (cm^{-1})	
	Fit	Calc.
0	−3.46(12)	−8.15
1	−7.53(15)	−10.2
2	−9.94(34)	−15.1
3	−29.36(58)	−44.7
4	15.4 (21)	15.5
5	—	7.2
6	—	−11.0

Note that only the e parity component of the $^1\Pi$ state is affected by this interaction. However, contributions to the energy shift can be positive or negative depending on the sign of the energy difference denominators in Eq. (16), which is determined by whether the $A^1\Sigma^+$ levels lie above or below the $A'^1\Pi$ state level of interest.

Table 8 compares the Λ-doubling constants for various $v_{A'}$ levels determined from our global fits with those calculated using Eq. (17). While the predicted values for the lower levels are somewhat larger than those determined from the fits, both the trend in magnitude and the abrupt change of sign from $v_{A'} = 3$ to $v_{A'} = 4$ is very well represented. This behaviour can readily be rationalized by the same types of arguments used in interpreting the predicted $b - A'$ shifts of Table 7. In particular, the predicted large magnitude of $q_{B1}(v_{A'} = 3)$ is explained by the fact that all contributions to the sum of Eq. (16) are negative and that the energy denominator associated with level $v_A = 0$ is relatively small (only $-165\,cm^{-1}$). Similarly, the change in sign for $v_{A'} = 4$ is due to the fact that the A-state level with the largest numerator matrix element both lies *below* $v_{A'} = 4$ and has a the smallest energy denominator of the terms in this sum ($-289\,cm^{-1}$).

Because the $A^1\Sigma^+$ state can only perturb the e parity levels of the $A'^1\Pi$ state, the rotational constant B_v^f in Eq. (18) would actually provide the best representation of the true "mechanical" B_v value. Note, however, that the conventional Λ-doubling formulation used to obtain the molecular constants given in Table 4 (see Eqs. (7)–(9)) differs from Eqs. (17) and (18). In particular, the constants in Table 4 were calculated using conventional effective rotational constants B_v^{eff}, defined such that,

$$B_v^e = B_v^{\text{eff}} + q_{1v}/2 \quad \text{and} \quad B_v^f = B_v^{\text{eff}} - q_{1v}/2. \tag{20}$$

4. Conclusions

Using a Broida-type oven source and a Fourier transform spectrometer, we recorded the $A'^1\Pi$–$X^1\Sigma^+$ near-infrared system of SrO at high spectral resolution, observing a total of 32 bands from ^{88}SrO, ^{87}SrO, ^{86}SrO for vibrational levels in the excited state extending from $v_{A'} = 0$ to 4. Over 5600 rovibrational lines were measured with an estimated precision of $0.005\,cm^{-1}$ and a maximum J value of 104. An improved set of X-state Dunham constants was obtained from a comprehensive combined-isotopomer least-squares fit of our new $A'^1\Pi$–$X^1\Sigma^+$ data together with the $A^1\Sigma^+$–$X^1\Sigma^+$ measurements of [18]. The $v_{A'} = 3$ and 4 vibrational levels of the $A'^1\Pi$ state were found to be much more strongly perturbed than $v_{A'} = 0 - 2$, due to both heterogeneous interaction with the $A^1\Sigma^+$ state and homogeneous interactions with the $b^3\Sigma^+$ state. Accordingly, they were represented as band constants in the global fit.

Prior to the present work, no high-resolution measurements of the $A'^1\Pi$–$X^1\Sigma^+$ system of SrO were available, so our results yield considerably improved spectroscopic constants for the $A'^1\Pi$ state. The previously reported constants described only high vibrational $A'^1\Pi$ state levels linked to the $v'' = 0$ or 1 level of the ground state, and provided only limited knowledge of the upper state. Moreover, no direct determination of the rotational constants was possible from those data, and it was only the inclusion of deperturbation results from the $A'^1\Pi \sim A^1\Sigma^+$ interaction in the $A^1\Sigma^+$–$X^1\Sigma^+$ system [10,11] which gave some approximate rotational constants. Although that combination of low resolution vibrational data and deperturbation information is more accurate than deperturbation results alone, it still provided only estimates of modest quality for the spectroscopic constants. Our direct measurement of over 5600 rovibrational lines provides a very precise description of the lower vibrational levels of the A' state.

A second aspect of this study concerns the improvement in ground state constants achieved by directly fitting all of the available high-resolution data for the two band systems simultaneously. Although, these constants are very similar to those listed in [18], and the predicted uncertainties are slightly larger, the improved statistics means that they will better represent the true magnitude and uncertainties of these quantities. Moreover, since data for the $A'^1\Pi$–$X^1\Sigma^+$ and $A^1\Sigma^+$–$X^1\Sigma^+$ systems were fitted together, the parameters listed in Tables 3 and 4 are optimum internally consistent values.

Using data from this work and from previous studies, RKR potentials for the $X^1\Sigma^+, A'^1\Pi, A^1\Sigma^+$ and $b^3\Sigma^+$ states have been generated, and Franck–Condon factors for the $A'^1\Pi$–$X^1\Sigma^+$ system are presented here. Since the $a^3\Pi, b^3\Sigma^+$, and $A^1\Sigma^+$ states all interact with and perturb the $A'^1\Pi$ state, Franck–Condon factors and matrix elements for the $b^3\Sigma^+ - A'^1\Pi$ and $A^1\Sigma^+ - A'^1\Pi$ systems were calculated and used in an effort to explain some of the observed perturbations. While the heterogeneous $A^1\Sigma^+ \sim A'^1\Pi$ interaction semi-quantitatively explains the observed Λ-doubling parameters for the $A'^1\Pi$ state,

we have been unable to rationalize apparent homogeneous shifts of +1.5 and +3.2 cm^{-1} in the fitted band origins for $v_{A'} = 3$ and 4, respectively. In order to confirm this and to further improve our understanding of the electronic structure in SrO, more extensive high-resolution measurements of the $a^3\Pi$ and $b^3\Sigma^+$ states are required. When such data becomes available, a full multi-state deperturbation of these overlapping electronic states will be possible.

Acknowledgments

This work was supported by the Natural Sciences and Engineering Research Council of Canada (NSERC). We thank R. Engleman for providing the strontium atomic line positions in advance of publication and W. Ernst for both his comments and for tracking down a typographical error in [37].

References

[1] R. Mecke, M. Guillery, Phys. Z. 28 (1928) 514–531.
[2] J. Querbach, Z. Phys. 60 (1930) 109.
[3] K. Mahla, Z. Phys. 81 (1933) 625.
[4] W.F. Meggers, Bur. Stand. J. Res. 10 (1933) 660.
[5] A. Lagerqvist, G. Almkvist, Arkiv für Fysik 22 (1949) 477–494.
[6] A. Lagerqvist, G. Almkvist, Arkiv für Fysik 23 (1950) 233–251.
[7] A. Lagerqvist, L. Selin, Arkiv für Fysik 22 (1956) 323–328.
[8] C.D. Jonah, R.N. Zare, C.H. Ottinger, J. Chem. Phys. 56 (1972) 263–274.
[9] F. Engelke, R.K. Sander, R.N. Zare, J. Chem. Phys. 65 (1976) 1146–1155.
[10] R.W. Field, J. Chem. Phys. 60 (1974) 2400–2413.
[11] G.A. Capelle, H.P. Broida, R.W. Field, J. Chem. Phys. 62 (1975) 3131–3137.
[12] J. Hecht, J. Chem. Phys. 65 (1976) 5026–5027.
[13] K. Schofield, T.M. Sugden, in: 1965 Symp. (Int.) Combust., 1965, p. 589.
[14] B.R. Rowe, J. Chem. Phys. 75 (1981) 3325–3325.
[15] W.B. England, J. Chem. Phys. 68 (1978) 4896–4900.
[16] I.G. Hermann, P.S. Wagener, The Oxide Cathode Volumes I and II, Chapman and Hall, 1951.
[17] C. Focsa, A. Poclet, B. Pinchemel, R.J. Le Roy, P.F. Bernath, J. Mol. Spectrosc. 203 (2000) 330–338.
[18] H. Li, R.H. Skelton, C. Focsa, B. Pinchemel, P.F. Bernath, J. Mol. Spectrosc. 203 (2000) 188–195.
[19] H. Li, C. Focsa, B. Pinchemel, R.J. Le Roy, P.F. Bernath, J. Chem. Phys. 113 (2000) 3026–3033.
[20] W.H. Hocking, E.F. Pearson, R.A. Creswell, G. Winnewisser, J. Chem. Phys. 68 (1978) 1128–1134.
[21] C.E. Blom, H.G. Hedderich, F.J. Lovas, R.D. Suenram, A.G. Maki, J. Mol. Spectrosc. 152 (1992) 109–118.
[22] C.R. Jones, H.P. Broida, J. Chem. Phys. 60 (1974) 4369–4376.
[23] P.R. Griffiths, J.A. de Haseth, Fourier Transform Infrared Spectrometry, Wiley, New York, 1986.
[24] B. Edlén, Metrologia 27 (1966) 1–80.
[25] K.P. Birch, M.J. Downs, Metrologia 30 (1993) 155–162.
[26] R. Engleman, private communication, 1999.
[27] R.J. Le Roy, DSParFit 2.0: A Computer Program for Fitting Multi-Isotopomer Diatomic Molecule Spectra, University of Waterloo Chemical Physics Research Report CP-653, 2001 (http://leroy.uwaterloo.ca).
[28] J.L. Dunham, Phys. Rev. 41 (1932) 721–731.
[29] G. Almkvist, A. Lagerqvist, Arkiv für Fysik 23 (1950) 233–251.
[30] N. Åslund, Arkiv für Fysik 30 (1965) 377–396.
[31] D.L. Albritton, W.J. Harrop, A.L. Schmeltekopf, R.N. Zare, E.L. Crow, J. Mol. Spectrosc. 46 (1973) 67–88.
[32] N. Åslund, J. Mol. Spectrosc. 50 (1974) 424–434.
[33] R.J. LeRoy, J. Mol. Spectrosc. 191 (1998) 221–223.
[34] R.J. Le Roy, RKR1: A Computer Program Implementing the First-Order RKR Method for Determining Diatom Potential Energy Curves from Spectroscopic Constants, University of Waterloo Chemical Physics Research Report CP-425, 1992 http://leroy.uwaterloo.ca).
[35] R.J. Le Roy, LEVEL 7.5: A Computer Program Solving the Radial Schrödinger Equation for Bound and Quasibound Levels, University of Waterloo Chemical Physics Research Report CP-655, 2002 (http://leroy.uwaterloo.ca).
[36] K.P. Huber, G. Herzberg, Constants of Diatomic Molecules, Van Nostrand, Princeton, NJ, 1979.
[37] (37) R.F.W. Herrmann, G.K. Sumnicht, M. Stein, W.E. Ernst, J. Mol. Spectrosc. 156 (1992) 487–500;
W. Ernst, private communication.
[38] M.W. Chase Jr., J.L. Curnutt, R.A. McDonald, A.N. Syverud, J. Phys. Chem. Ref. Data 7 (1978) 793, JANAF Thermochemical Tables, 1978 supplement.
[39] H. Partridge, S.R. Langhoff, C.W. Bauschlicher Jr., Chem. Phys. Lett. 121 (1985) 163–168.
[40] J. Schamps, H. Lefebvre-Brion, J. Chem. Phys. 56 (1972) 573–585.
[41] K.D. Carlson, K. Kaiser, C. Moser, A.C. Wahl, J. Chem. Phys. 52 (1970) 4678–4691.
[42] W.M. Huo, K.F. Freed, W. Klemperer, J. Chem. Phys. 46 (1967) 3556–3565.
[43] S.R. Rice, H. Martin, R.W. Field, J. Chem. Phys. 11 (1985) 5023–5034.
[44] D.P. Baldwin, E.J. Hill, R.W. Field, J. Am. Chem. Soc. 112 (1990) 9156–9161.
[45] H. Lefebvre-Brion, R.W. Field, Perturbations in the Spectra of Diatomic Molecules, Academic Press, New York, 1986.